ISSN 1070-3284, Russian Journal of Coordination Chemistry, 2014, Vol. 40, No. 8, pp. 565–570. © Pleiades Publishing, Ltd., 2014.
Original Russian Text © I.A. Martynova, D.M. Tsymbarenko, N.P. Kuz'mina, 2014, published in Koordinatsionnaya Khimiya, 2014, Vol. 40, No. 8, pp. 494–500.

# Yttrium Tris-Propionate Monohydrate: Synthesis, Crystal Structure, and Thermal Stability

**I. A. Martynova, D. M. Tsymbarenko, and N. P. Kuz'mina**

*Moscow State University Moscow, 119899 Russia*

**e-mail: irinamartynova87@gmail.com*

Received October 30, 2013

**Abstract**—The complex $[Y(Prop)_3(H_2O)]_\infty$ (**I**) was prepared by treating yttrium carbonate, acetate, or acetylacetonate hydrates with propionic acid and characterized by the data of elemental analysis, IR spectroscopy, X-ray diffraction, and thermal analysis in air. Complex **I** has a polymeric layered structure with clear-cut structure-forming dimeric groups bridged by bidentate ligands. Only van der Waals interactions occur between the adjacent polymeric layers. In air, yttrium propionate monohydrate **I** is completely converted to the oxide at 600°C.

**DOI:** 10.1134/S1070328414080077

## INTRODUCTION

Metal-organic coordination compounds (CC) play an important role in modern material science. There are two key modes of application of CC to the design of new materials: preparation of materials with functional properties of CC and synthesis of inorganic or hybrid materials by chemical transformations of CC serving as precursors. The demand of new materials often initiates synthesis of new CC or vigorous research of known but poorly studied compounds. For example, metal propionates have been known for a long time but have not been systematically investigated.

The increased interest in metal propionates is due to their use as precursors for the production of thin films of oxide materials by metal-organic chemical solution deposition (MOCSD). The essence of this method is to prepare solutions of metal-organic precursors containing the elements required for the material in the appropriate stoichiometry, deposition of the precursor films on the substrate, and subsequent transformation of the films into functional layers upon heat treatment and annealing under appropriate conditions [1]. Currently this method is being vigorously developed as applied to the technology of second-generation high-temperature superconducting (HTSC) ribbons, which are complex textured heterostructures composed of functional layers on extended metallic (nickel alloy) substrates (ribbons) [2]. In the MOCSD production of $La_2Zr_2O_7$ buffer layers, propionic acid (HProp) was proposed for the first time as an efficient solvent [3]. Advantages of this solvent include viscosity (1.102 mPa · s) that ensures film deposition, good wetting of the substrates, and the possibility to prepare concentrated (0.2–0.6 mol/L) solutions stable against precipitation during long-term storage and use. Propionic acid has been successfully used for the deposition by MOCSD of thin films of not only $La_2Zr_2O_7$ [3–5] but also $La_2O_3$ [6], $CeO_2$ [7], ZnO [8], and complex oxides containing CuO [9–11] or BaO [9–12]. The starting compounds for propionate precursors are, most often, the appropriate metal acetylacetonates or acetates, which react with HProp in solutions to give metal propionates or mixed-ligand complexes. In the MOCSD method, the composition and properties of the precursors are important for their transformation into the final product. Therefore, determination of the composition, structure, and thermal stability of propionates existing in the solution of precursors is a fairly topical task. Some recent publications describe the structure and the thermal stability of the CC isolated from solutions of propionate precursors, namely, $\{[Zr_6O_8(Prop)_8(CH_3COO)_4](CH_3COOH)(HProp)\}_2$ [13], $[Zr_6O_4(OH)_4(Prop)_{12}]_2$ [14], $[Ba_7(Prop)_{10}(CH_3COO)_4 \cdot 5H_2O]$ [15], and $[Cu(Prop)_2] \cdot 2H_2O$ [16].

The crystal structures of propionates of some light lanthanides were determined, namely, for $\{[La_2(Prop)_6(H_2O)_3] \cdot 3.5H_2O\}_\infty$ [6], $[Pr_2(Prop)_6(H_2O)_3)]_\infty$ [17], and $[Nd_2(Prop)_6(HProp)_2]_\infty$ [18]. The thermolysis process of lanthanum and cerium propionates, which are parts of precursors for deposition of buffer oxide layers, has been studied in detail [6, 7]. Propionates of the yttrium group lanthanides are also of interest as precursors of functional materials, first of all, $Y_2O_3$ [19, 20]; therefore, publications considering the synthesis and thermal stability of $[Ln(Prop)_3(H_2O)]$ (Ln = Ho, Er, Tm, Yb [21], Y [22, 23], and Lu [24]) appeared. Virtually no data on the structures of yttrium group lanthanide propionates were reported. A model of the structure of yttrium propionate $\{[Y_2(Prop)_6(H_2O)]\}_\infty$ based on quantum chem-

**Table 1.** Crystal data and X-ray experiment and structure refinement details for structure **I**

| Parameter | Value |
|---|---|
| $M$ | 652.27 |
| System, space group | Triclinic; $P\bar{1}$ |
| $a$, Å | 9.619(3) |
| $b$, Å | 12.116(4) |
| $c$, Å | 13.181(5) |
| α, deg | 66.201(6) |
| β, deg | 68.823(6) |
| γ, deg | 89.882(6) |
| $V$, Å$^3$ | 1292.0(8) |
| $Z$ | 4 |
| $\rho_{calc}$, g · cm$^{-3}$ | 1.677 |
| μ, mm$^{-1}$ | 4.53 |
| $F$(000) | 664 |
| Crystal size, mm | 0.76 × 0.22 × 0.14 |
| Scan mode | φ–ω |
| θ Range, deg | 1.84 ≤ and ≤ 29.00 |
| Range of indices | $-13 \le h \le 12$, $-16 \le k \le 16$, $-14 \le l \le 17$ |
| Number of measured reflections | 20174 |
| Number of independent reflections ($R_{int}$) | 6789 (0.091) |
| Number of reflections with $I > 2\sigma(I)$ | 4189 |
| Number of refined parameters | 313 |
| $R$ ($F^2 > 2\sigma(F^2)$), | 0.091 |
| $wR$ ($F^2$) | 0.279 |
| GOOF | 1.02 |
| $T_{max}$, $T_{min}$ | 0.531, 0.280 |
| $\Delta\rho_{min}/\Delta\rho_{max}$, $e$ Å$^{-3}$ | −3.11/6.29 |

ical modeling of only one molecular fragment was described [22].

In this work, the propionate $[Y(Prop)_3(H_2O)]_\infty$ (**I**) was prepared by the reaction of HProp with yttrium carbonate, acetate, or acetylacetonate and characterized by elemental analysis, IR spectroscopy, and powder X-ray diffraction. Its crystal structure was solved for the first time.

## EXPERIMENTAL

Reagent grade $Y(Acac)_3 \cdot 3H_2O$, $Y_2(CO_3)_3 \cdot 3H_2O$, $Y(OAc)_3 \cdot 4H_2O$, and HProp were used as the starting compounds. The syntheses were carried out in propionic acid, which served as a solvent.

The reactions of yttrium carbonate, acetate, or acetylacetonate (3 mmol) with HProp (15 mL, 200 mmol) with heating (70–80°C) gave transparent reaction mixtures. On cooling, crystalline precipitates of **I** were formed. Yield ~90%.

According to elemental and powder X-ray diffraction analysis, the composition of the obtained precipitates was the same for any of the starting yttrium compounds (the powder X-ray diffraction data are not presented in the paper). In the synthesis from $Y(Acac)_3 \cdot 3H_2O$, single crystals of **I** suitable for X-ray diffraction were isolated.

| For $C_9H_{17}O_7Y$ | | | |
|---|---|---|---|
| anal. calcd., %: | C, 33.1; | H, 5.2; | Y, 27.3. |
| Found, %: | C, 33.2; | H, 5.4; | Y, 27.8. |

IR (ν, cm$^{-1}$): 3158 ν(OH), 1661 δ(OH), 1588, 1558, 1538 $\nu_{as}(COO^-)$, 1464, 1442, 1413 $\nu_s(COO^-)$, 1288 $\nu(CH_2)$.

Analysis of the samples for C and H was performed using a C,H,N-microanalyzer of the Chair of Organic Chemistry at the Department of Chemistry, Lomonosov Moscow State University; yttrium was determined by complexometric titration [25].

The IR spectra of the solid samples were recorded in the frustrated total internal reflection mode on a Perkin Elmer Spectrum One FT-IR instrument at 4000–650 cm$^{-1}$.

Powder X-ray diffraction analysis was performed in the Guinier–Johansson monochromator, Enraf–Nonius FR552 instrument (Ge monochromator, Cu$K_{\alpha 1}$ radiation, λ = 1.540598 Å).

Thermal analysis was performed on a Derivatograph Q1500D in the 30–1000°C range in air (10°C/min heating rate, 45 mg weighed portion, alundum crucible).

**X-ray diffraction analysis** was done on a Bruker Smart APEX2 CCD diffractometer (λ(Mo$K_\alpha$) = 0.71072 Å, graphite monochromator) at 100 K. The structure was solved by direct methods followed by Fourier syntheses and refined by the full-matrix least-squares method in the anisotropic approximation for all non-hydrogen atoms. The positions of hydrogen atoms of the $CH_2$- and $CH_3$ groups were calculated geometrically and refined in the riding model with specified isotropic thermal parameters. For all calculations, the SHELXTL PLUS 5.0 program package was used [26]. The absorption corrections were applied using the SADABS program [27]. Selected crystallographic parameters are presented in Table 1. The full set of crystallographic data for the structure

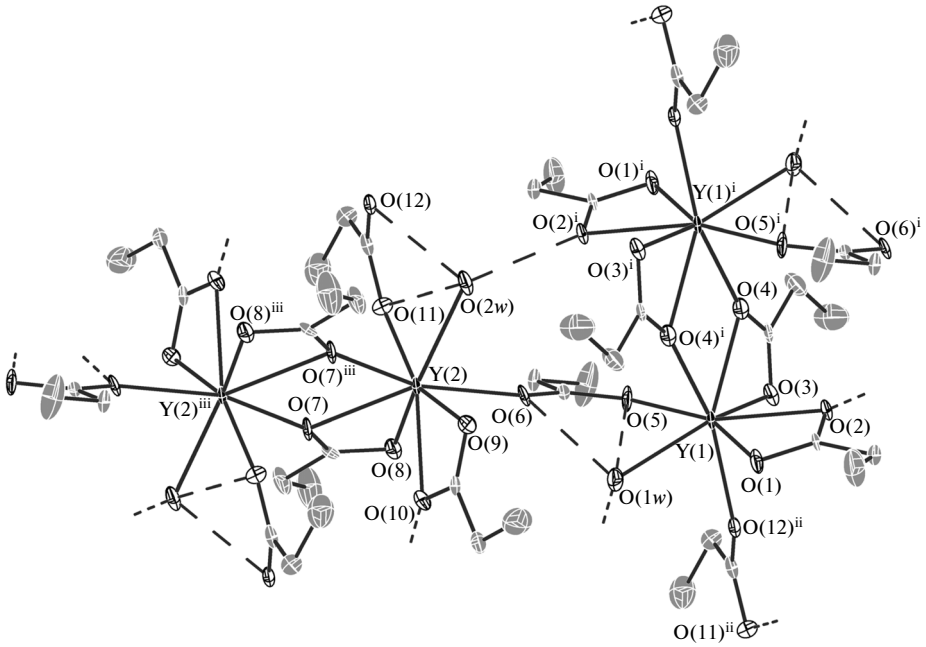


**Fig. 1.** Dimeric fragments in the crystal structure of **I**.

of **I** has been deposited at the Cambridge Crystallographic Data Centre (no. 969363; deposit@ccdc.cam.ac.uk; http://www.ccdc.cam.ac.uk/data_request/cif).

## RESULTS AND DISCUSSION

Yttrium propionate was synthesized using both the traditional method, namely, the reaction of yttrium carbonate and acetate with propionic acid [28] and also the reaction of HProp with yttrium acetylacetonate (β-diketonate), which is used to prepare precursors [3]. Irrespective of the initial yttrium compound, all of the syntheses gave the crystalline precipitate of **I** having a solubility in HProp less than 0.2 mol/L. The experimental X-ray diffraction patterns of all products **I** were identical and consistent with that calculated for **I** from single crystal X-ray diffraction data.

The asymmetric part of the unit cell of **I** contains two yttrium atoms (Y(1), Y(2)), two sets of propionate anions with chelating (O(1), O(2), O(9), O(10)), chelating-bridging (O(3), O(4), O(7), O(8)), and bridging (O(5), O(12), O(6), O(11)) structural fragments, and two coordination water molecules (O(1*w*), O(2*w*)) (Fig. 1).

The crystal structure of **I** is layered. The layers are formed by alternating centrosymmetrical dimeric fragments $\{Y(1)_2(Prop)_6(H_2O(1w))_2\}$ and $\{Y(2)_2(Prop)_6(H_2O(2w)_2\}$. The dimeric fragments have identical structures and differ only by the orientation relative to the crystallographic axes (Fig. 2). The bond lengths and bond angles for yttrium bonds with the ligands having the same structural functions differ by not more than 2% (Table 2).

In the dimers $\{Y_2(Prop)_6(H_2O)_2\}$, yttrium atoms are linked by two tridentate chelating-bridging propionate ligands. The dimeric fragments are joined into a polymeric network within the layer by bidentate bridging ligands (Fig. 1). Each yttrium ion coordinates eight oxygen atoms, specifically, three atoms of the tridentate chelating-bridging ligand, two atoms of the bidentate chelating ligand, two atoms of two bidentate bridging ligands, and one oxygen atom of the water molecule (Fig. 1). The coordination polyhedra of yttrium are distorted two-cap trigonal prisms, which is typical of lanthanide carboxylates with C.N. = 8 [29].

In the tridentate chelating-bridging ligands, the average Y–O bond length (2.424(2) Å) is longer than the bridging bonds (average 2.284(16) Å). This relationship between these bond lengths is typical of lanthanide carboxylates [30, 31]. The average Y–O bond length in the bidentate chelating ligands is 2.382 Å. The average length of the Y–O(*w*) bond with the water oxygen atoms (2.379(7) Å) is close to the bond lengths in the chelate rings. The average d(Y–O) distance to the oxygen atoms of the interdimer bridging carboxylate groups is 2.283 Å.

The average Y–Y distance in the dimers is much shorter than the distance between the yttrium ions of the neighboring dimers (3.9017(2) and 6.144(4) Å, respectively), which makes the polymeric structure of **I** unique. Substantial differences between the bond lengths within and between the dimeric fragments are more characteristic of molecular structures composed of isolated dimers. For example, in the molecular

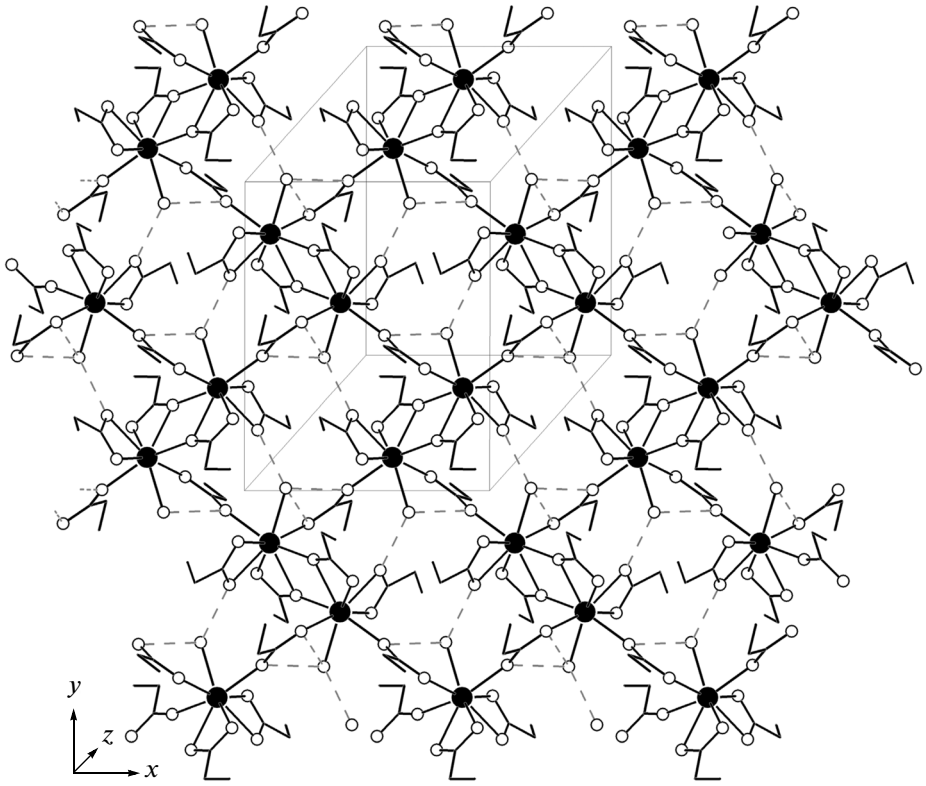


**Fig. 2.** Fragment of the polymeric layer in the crystal structure of **I**.

structure $\{[Y(OAc)_3(H_2O)_2](H_2O)_4\}$ where the yttrium coordination number is 9, the average Y(1)–Y(1) distance inside the dimers is 4.129 Å, while that between the dimers is 6.398 Å. In the polymeric chain-like crystal structure $[Y(OAc)_3(H_2O)_{0.5}]_\infty$, the yttrium ions are connected by two tridentate chelating-bridging and one bidentate bridging acetate groups and the yttrium –yttrium distances are 3.993 and 3.950 Å.

The crystal structure of **I** consists of polymeric layers facing one another by non-polar ethyl groups of the propionate ligands. Only van der Waals interactions occur between the neighboring polymeric layers.

The two types of dimers are arranged in the chessboard fashion forming a herringbone packing (Fig. 2). This packing is additionally stabilized by a water molecule due to the hydrogen bond system formed within the layer. The water protons were not located; however, considering the oxygen–oxygen distances, it can be inferred that each water molecule forms three (two weak and one medium-strength) hydrogen bonds (Table 2).

The crystal structure of **I** differs from the known structures of lanthanide propionates (derived from light lanthanides), which is obviously related to the different ionic radii and the possibility of large coordination numbers in compounds of light lanthanides.

The crystals of lanthanum $\{[La_2(Prop)_6(H_2O)](H_2O)_{3.5}\}$ and praseodymium $\{[Pr_2(Prop)_6(H_2O)_3] \cdot (H_2O)_3\}$ propionate hydrates are isostructural and form zigzag chains in which central ions with different coordination environments (C.N. 9 or 10) alternate. The neighboring Ln(1)–Ln(2) ions are joined by a pair of tridentate chelating-bridging propionate groups. The Ln(1)–Ln(2) and Ln(2)–Ln(1) bond lengths are 4.373 and 4.378 Å (for $\{[La_2(Prop)_6(H_2O)](H_2O)_{3.5}\}$) and 4.337 and 4.348 Å (for $\{[Pr_2(Prop)_6(H_2O)_3] \cdot (H_2O)_3\}$), respectively. The $[Y_2(Prop)_6(H_2O)]$ semihydrate model [22] is based on the motif detected in the polymeric semihydrate structure $[Y(OAc)_3(H_2O)_{0.5}]_\infty$, namely, the Y(1) and Y(2) ions with C.N. of 9 and 8 are connected to polymeric chains by two tridentate chelating-bridging and one bidentate bridging ligand. The Y(1) ion coordinates the oxygen atom of the water molecule. The proposed model seems unreliable because the fact of yttrium propionate formation as a semihydrate has been confirmed by neither elemental nor thermal analysis data. Monohydrate appears to be the most stable form for yttrium group lanthanide propionates. This is indicated by the reported data [21–24] and our results.

The IR spectrum of **I** exhibits characteristic absorption bands typical of lanthanide carboxylates. Indeed, a broadened band in the range of 3300–3100 $cm^{-1}$ is related to the ν(OH) stretching mode, indicating that a water molecule is present in the salt. This is confirmed by the δ(OH) band at 1661 $cm^{-1}$.

**Table 2.** Selected geometric parameters of the structure of **I***

| Bond | *d*, Å | Bond | *d*, Å | Valence angle | ∠, deg |
|---|---|---|---|---|---|
| Bidentate chelating ligand | | | | | |
| Y(1)–O(1) | 2.385(6) | Y(2)–O(9) | 2.392(6) | O(1)Y(1)O(2) | 54.8(2) |
| Y(1)–O(2) | 2.381(7) | Y(2)–O(10) | 2.373(6) | O(9)Y(1)O(10) | 54.5(2) |
| Tridentate chelating-bridging ligand | | | | | |
| Y(1)–O(3) | 2.421(6) | Y(2)–O(7) | 2.423(5) | O(3)Y(1)O(4) | 53.6(2) |
| Y(1)–O(4) | 2.420(6) | Y(2)–O(8) | 2.432(7) | Y(1)O(4)Y(1)$^{i}$ | 112.0(2) |
| Y(1)–O(4)$^{i}$ | 2.285(9) | Y(2)–O(7)$^{iii}$ | 2.289(6) | O(7)Y(2)O(8) | 53.5(2) |
| | | | | Y(2)O(7)Y(2)$^{iii}$ | 111.8(3) |
| Bridging ligand | | | | | |
| Y(1)–O(5) | 2.302(6) | Y(2)–O(6) | 2.259(5) | O(5)C(7)O(6) | 122.0(8) |
| Y(1)–O(12)$^{ii}$ | 2.276(6) | Y(2)–O(11) | 2.295(6) | O(11)C(16)O(12) | 122.0(8) |
| Water molecule | | | | | |
| Y(1)–O(1*w*) | 2.377(6) | Y(2)–O(2*w*) | 2.380(8) | | |
| D–H···A | | D···A, Å | D–H···A | | D···A, Å |
| O(1*w*)–H···O(5) | | 2.855(7) | O(2*w*)–H···O(11) | | 2.863(2) |
| O(1*w*)–H···O(6) | | 2.861(8) | O(2*w*)–H···O(12) | | 2.812(8) |
| O(1*w*)–H···O(10)$^{iv}$ | | 2.698(2) | O(2*w*)–H···O(2)$^{i}$ | | 2.712(8) |

* Symmetry codes: $^{i}$ $1-x, -y, 1-z$; $^{ii}$ $1+x, y, z$; $^{iii}$ $-x, 1-y, 1-z$; $^{iv}$ $1-x, 1-y, 1-z$.

The carboxylate stretching bands $\nu_{as}(COO^-)$ and $\nu_s(COO^-)$ occur at 1590–1525 $cm^{-1}$ and 1470–1410 $cm^{-1}$, respectively. Splitting of the asymmetric and symmetric COO stretching bands into three components is in good agreement with the X-ray diffraction data indicating several structural functions of the propionate ligands.

The data on the thermal behavior of yttrium propionate are limited to the study of the thermolysis under argon [22]. We performed thermal analysis of **I** in air (Fig. 3). In the thermogram of **I**, the first mass loss stage at 60–110°C corresponds to the elimination of the coordinated water molecule ($\Delta m_{calc}$ = 5.5%; $\Delta m_{exp}$ = 5.4%). In the TG curve (Fig. 3), it is difficult to separate the second and third stages (175–525°C) corresponding to the major decomposition of anhydrous yttrium propionate to the oxide (total $\Delta m_{calc}$ = 65.3%; $\Delta m_{exp}$ = 65.4%). The presence of two minima in the DTG curve (~300 and 380°C) attests to the decomposition of yttrium propionate via the formation of the oxocarbonate $Y_2O_2CO_3$. As a whole, the course of thermolysis of **I** is in line with data on decomposition of lanthanide acetates [32], $\{[Y_2(Prop)_6(H_2O)] \cdot 3.5H_2O\}_\infty$ [22] in air and $[Y(Prop)_3(H_2O)]$ [23] in an inert atmosphere. In air, the transformation of yttrium propionate **I** to the oxide is completed at 600°C.

In conclusion, we would like to note the following. Treatment of yttrium carbonate, acetate, or acetylacetonate hydrate with propionic acid results in the formation of propionate $[Y(Prop)_3(H_2O)]_\infty$ (**I**), which was studied by X-ray crystallography. The structure of **I** is a unique example of a polymeric layered lanthanide carboxylate with clearly defined dimeric structure-forming fragments connected by bidentate bridging ligands. To our knowledge, structures of this type have not been described previously for lanthanide carboxylates. In air, transformation of yttrium propionate **I** into the oxide is completed at 600°C, i.e., as regards thermal stability in air, compound **I** corresponds to requirements to precursors of oxide materials. How-

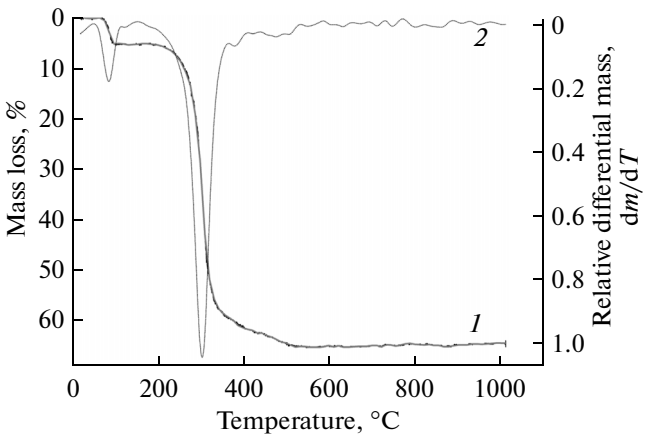


**Fig. 3.** (*1*) TG and (*2*) DTG curves for **I** in air.

ever, the solubility of **I** in propionic acid does not exceed 0.2 mol/L, which may restrict the broad use of solutions of **I** in HProp as precursors for MOCSD.

## ACKNOWLEDGMENTS

The authors are grateful to the X-ray Structural Center of the Nesmeyanov Institute of Organoelement Compounds and particularly to K.A. Lysenko for providing the possibility to perform X-ray diffraction analysis.

This work was supported by the Russian Foundation for Basic Research (project no. 11-03-01208-a).

## REFERENCES

1. Bhuniyan, M.S., Paranthaman, M., and Salma, K., *Supercond. Sci. Technol.*, 2006, vol. 19, p. R1.
2. Goyal, A., *Second-Generation HTS Conductors*, New York: Boston, Dordrecht, London, Moscow: Kluwer Academic, 2005.
3. Engel, S., Hühne, R., Knoth, K., et al., *J. Cryst. Growth*, 2008, vol. 310, p. 4295.
4. Knoth, K., Hühne, R., Oswald, S., et al., *Thin Solid Films*, 2008, vol. 516, p. 2099.
5. Li, C.S., Yu, Z.M., Odier, P., et al., *Physica C*, 2011, vol. 471, p. 974.
6. Ciontea, L., Nasui, M., Petrisor, T., Jr., et al., *Mater. Res. Bull.*, 2010, vol. 45, p. 1203.
7. Ciontea, L., Ristoiu, T., Mos, R.B., et al., *Mater. Chem. Phys.*, 2012, vol. 133, p. 772.
8. Mereu, R.A., Mesaros, A., Petrisor, T., Jr., et al., *J. Anal. Appl. Pyrol.*, 2012, vol. 97, p. 137.
9. Armenio, A.A., Augieri, A., Ciontea, L., et al., *Supercond. Sci. Technol.*, 2008, vol. 21, p. 125015.
10. Armenio, A.A., Celentano, G., Rufoloni, A., et al., *IEEE Trans. Appl. Supercond.*, 2009, vol. 19. p. 3204.
11. Ciontea, L., Angrisani, A., Celentano, G., et al., *J. Phys. Conf. Ser.*, 2008, vol. 97, p. 012302-1.
12. Mos, R.B., Gabor, M.S., Nasui, M., et al., *Thin Solid Films*, 2010, vol. 518, p. 4714.
13. Petit, S., Morlens, S., Yu, Z., et al., *Solid State Sci.*, 2011, vol. 13, p. 665.
14. Mos, R.B., Nasui, M., Petrisor, T., Jr., et al., *J. Anal. Appl. Pyrol.*, 2012, vol. 97, p. 137.
15. Mos, R.B., Nasui, M., Petrisor, T., Jr., et al., *J. Anal. Appl. Pyrol.*, 2011, vol. 92, no. 2, p. 445.
16. Nasui, M., Mos, R.B., Petrisor, T., Jr., et al., *J. Anal. Appl. Pyrol.*, 2011, vol. 92, p. 439.
17. Deiters, D. and Meyer, G., *Z. Anorg. Allg. Chem.*, 1996, vol. 622, p. 325.
18. Torres, S.G., *PhD Thesis*, Köln, 2007.
19. Martynova, I., Tsymbarenko, D., Kamenev, A., et al., *Physica E*, 2014, vol. 56, no. 1, p. 447.
20. Sheehan, C., Jung, Y., Holesinger, T., et al., *Appl. Phys. Lett.*, 2011, vol. 98, pp. 071907-1.
21. Grivel, J.-C., *J. Therm. Anal. Calorim.*, 2012, vol. 109, p. 81.
22. Nasui, M., Bogatan, C., Ciontea, L., et al., *J. Anal. Appl. Pyrol*, 2012, vol. 97, p. 88.
23. Grivel, J.-C., *J. Anal. Appl. Pyrol.*, 2013, vol. 101, p. 185.
24. Grivel, J.-C., *J. Anal. Appl. Pyrol.*, 2010, vol. 89, p. 250.
25. Prisibl, R., *Complexones in Chemical Analysis* [Russian Translation], Moscow: Mir, 1955.
26. Sheldrick, G.M., *SHELXTL. Version 5.10. Structure Determination Software Suite*, Madison (WI, USA): Bruker AXS, 1998.
27. Sheldrick, G.M., *SADABS. Version 2.01. Bruker/Siemens Area Detector Absorption Correction Program*, Madison (WI, USA): Bruker AXS, 1998.
28. Gmelin, L., *Handbook of Inorganic Chemistry. D5. Carboxylates*, Berlin, Heidelberg, New York, Tokyo, 1984.
29. Ouchi, A., *Coord. Chem. Rev.*, 1988, vol. 92, p. 29.
30. Junk, P.C., Kepert, C.J., Wei-Min, L., et al., *Aust. J. Chem.*, 1999, vol. 52, p. 437.
31. Martynenko, L.I., Kuz'mina, N.P., and Grigor'ev, A.N., *Ross. Khim. Zh.*, 1996, vol. 40, p. 110.
32. Patil, K.C., Chandrashekhma, G.V., Georgea, R., et al., *Can. J. Chem.*, 1968, vol. 46, p. 257.

*Translated by Z. Svitanko*